Broadside-Coupled Coplanar Waveguides and Their End-Coupled Band-Pass Filter Applications

Cam Nguyen, *Senior Member, IEEE*

Abstract—**New broadside-coupled coplanar waveguides, suitable for applications requiring wide bandwidths, tight couplings, and large mode effective-dielectric-constant ratios, are presented. Their analysis and investigation are described. Simple equations relating the per-unit-length capacitances of the c- and π-modes and the per-unit-length capacitance matrices of the coupled structures to those obtained when applying even- and odd-symmetric voltages are also derived. New broadside end-coupled band-pass filters have been developed at X-band (8–12 GHz) with less than 1.5 and 1.0 dB passband insertion losses using the proposed four-ground-plane and two-ground-plane coplanar waveguide structures, respectively. Good agreement between the experimental results and those predicted theoretically was also observed.**

I. Introduction

EDGE-COUPLED parallel transmission lines are very useful transmission media for many microwave components such as filters and couplers. The main drawback of these structures is the weak coupling that results in limited operating bandwidths. A novel broadside-coupled structure, first proposed by Dalley [1] using strip-line technique and subsequently investigated by Allen and Estes [2], has an inherent broad-band characteristic. The wide-band feature is obtained from the strong coupling produced by the two broadside-coupled strips. As pointed out in [3], this structure also has several desirable features not achievable by its edge-coupled counterpart, such as multiple stop-band and multizero pass-band responses from a single filter section, due to the large ratio between the even- and odd-mode phase velocities. A similar structure realized using coplanar waveguide (CPW) transmission line would be an attractive candidate for both microwave integrated circuit (MIC) and microwave monolithic integrated circuit (MMIC) applications. The use of CPW for MICs and MMICs has recently been growing due to its many appealing properties, including 1) elimination of via holes in connecting circuit elements to ground, 2) easy realizations of compact baluns for balanced circuits, and 3) good line-to-line isolation.

A symmetrical broadside-coupled CPW, with air above and below the substrate, was first proposed and analyzed by Hatsuda [4]. Another version of broadside-coupled CPW with equally thick dielectric materials above and below the main substrate, sandwiched between top and bottom conducting covers, has also been analyzed [5]. In these structures, four ground planes on both sides of the main substrate are used. These ground planes form a parallel-plate waveguide that can produce leakage loss in the structure due to coupling to the parallel-plate mode. In addition, higher-order waveguide modes may be generated if all four planes are not kept at the same RF potential. Maintaining the same RF potential for all these ground planes is extremely difficult, if not impossible, at high microwave frequencies. These undesired parallel-plate and higher-order mode propagations excite spurious resonances and unwanted couplings, which limit and degrade circuit performance. The operating frequency range of these broadside-coupled CPWs are thus limited.

To overcome the problems of leakage loss and higher-order mode propagations, we have modified the reported structures [4], [5], by using an enclosed conducting channel and different thicknesses for regions above and below the main substrate, and proposed a new one that has only two ground planes located on the same side of the substrate, as depicted in Fig. 1. The modified and new broadside structures can avoid leakage of energy and propagations of higher-order modes up to high frequencies with appropriate channel dimensions and substrate parameters, and thus extend the operating frequency range. The new version, especially, eliminates the parallel-plate mode propagation and excites less higher-order modes due to the use of only two ground planes on the same substrate side, which can easily be maintained at the same RF potential, and thus further increases the operating frequency limits. In addition, it has lower loss due to the use of wider center conductors for given characteristic impedances, substrate thicknesses, and dielectric constants and less conductor-edge loss as compared with that for the modified structure. Moreover, our proposed structures can have improved characteristic impedance ranges by proper selection of spacings between the main substrate and the top and bottom channel walls. Finally, as compared to the broadside-coupled strip-line, the new transmission lines have additional desirable features provided by the gaps, including more design flexibility and large impedance range.

In this paper, we present the analysis and detailed investigation of these new broadside-coupled CPWs (Figs.

Manuscript received March 31, 1992; revised July 28, 1992. This work was supported in part by the NASA Center for Space Power.

The author is with Electromagnetics and Microwave Laboratory, Department of Electrical Engineering, Texas A&M University, College Station, Texas 77843-3128.

IEEE Log Number 9203688.

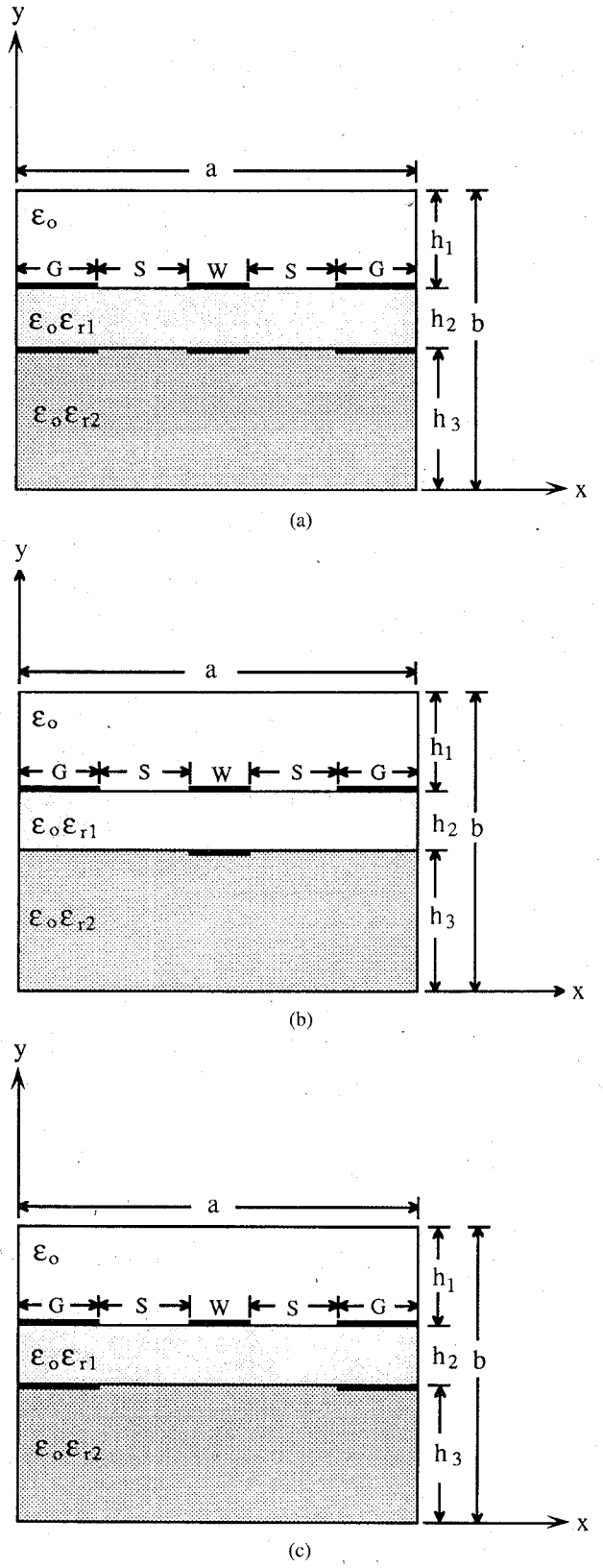

Fig. 1. Cross sections of the FBCPW (a), TBCPW (b) and single CPW (c).

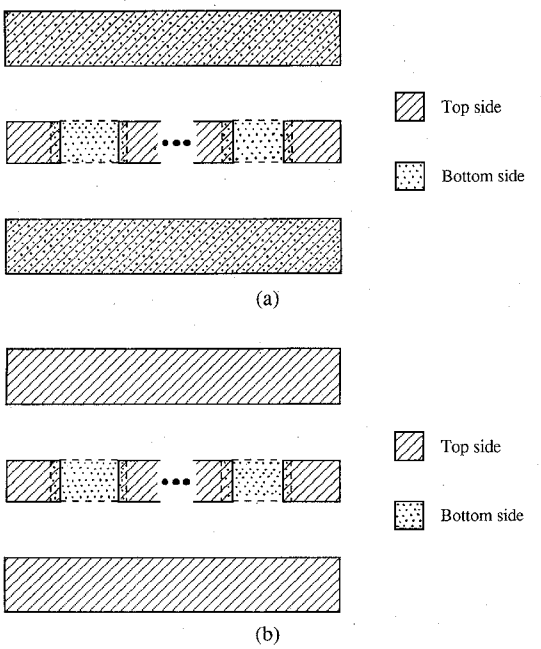

Fig. 2. CPW broadside end-coupled band-pass filters using FBCPW (a) and TBCPW (b).

1(a), (b)): the four-ground-plane (FBCPW) and two-ground-plane (TBCPW) broadside-coupled CPWs, whose ground planes are located on the substrate surfaces. The analysis is based on the quasi-static spectral domain approach (SDA) developed by Itoh [6]. New and simple equations relating the capacitances per unit length of the c and π propagation modes and the elements of the per-unit-length capacitance matrices to those obtained when applying even- and odd-symmetric voltages are derived. Various numerical results for the mode characteristic impedances and effective dielectric constants of the new broadside-coupled CPWs are presented and discussed.

In comparison with the popular microstrip line, filter development on CPW has been very sporadic, in spite of its attractive advantages. Only a few CPW filters have been reported, such as the CPW end-coupled band-pass filters [7], CPW short-circuited stub band-stop filters and open-circuited stub band-pass filters [8], and CPW-slot line band-pass filters [9].

In this paper, we also report, for the first time, the development of new end-coupled band-pass filters using the proposed broadside-coupled CPWs (Fig. 2). Compared to the conventional CPW end-coupled filter [7], this filter structure can achieve the tight coupling between resonator elements required for wide-band applications. The characteristic impedance and effective dielectric constant for the single CPW (Fig. 1(c)), employed in the filters, are also obtained using the quasi-static SDA. Two X-band (8–12 GHz) three-section end-coupled band-pass filters, employing the proposed broadside structures, have been built and tested, and measured performances agree favorable with the results calculated theoretically.

II. Formulation

Fig. 1 shows cross sections of the considered broadside-coupled and single CPWs. The structures are enclosed in a perfectly conducting waveguide and assumed to be uniform and infinite in the z-direction. Both the

ground planes and central strips are assumed to be perfectly conducting and infinitesimally thin, and the dielectric substrates are assumed to be lossless. These broadside-coupled structures support two quasi-TEM propagation modes, the c-mode (in-phase) and the π-mode (anti-phase), similar to those in the two asymmetric parallel coupled lines embedded in an inhomogeneous medium [10]. The c- and π-modes become the even- and odd-modes when $h_1 = h_3$ and $\epsilon_2 = \epsilon_0$ for the FBCPW. The analyses for these structures are similar, except that there exists only a single quasi-TEM mode in the single CPW structure. So only that of the FBCPW is described. The analysis consists of two parts. First, we use the quasi-static SDA [6] to obtain the capacitances per unit length corresponding to equal (even-symmetric) and opposite (odd-symmetric) potential excitations. Second, we evaluate the capacitances per unit length and then the characteristic impedances and effective dielectric constants for the c- and π-modes.

A. Even- and Odd-Mode Quasi-Static Analysis

We begin the analysis by defining a Fourier transform with respect to x as

$$\tilde{f}(\alpha_n, y) = \frac{2}{a}\int_0^a f(x, y)\sin \alpha_n x\, dx \tag{1}$$

where the tilda ($\sim$) specifies the Fourier-transformed quantity and $\alpha_n = n\pi/a$, $n = 1, 2, \cdots$, is the Fourier-transform variable. The unknown potentials $\tilde{\phi}_i(\alpha_n, y)$, $i = 1, 2, 3$, in region i are the solutions of the Fourier-transformed Laplace equation

$$\frac{d^2\tilde{\phi}_i(\alpha_n, y)}{dy^2} - \alpha_n^2\tilde{\phi}_i(\alpha_n, y) = 0 \tag{2}$$

which are found to be

$$\tilde{\phi}_1(\alpha_n, y) = A\sinh \alpha_n(b - y) \tag{3a}$$

$$\tilde{\phi}_2(\alpha_n, y) = B\sinh \alpha_n(y - h_3) + C\cosh \alpha_n(y - h_3) \tag{3b}$$

$$\tilde{\phi}_3(\alpha_n, y) = D\sinh \alpha_n(y) \tag{3c}$$

where A, B, C, and D are unknown functions of α_n. The boundary conditions at the perfectly conducting walls at $x = 0, a$ and at $y = 0, b$ are already enforced in the above potential functions. The remaining boundary conditions in the spectral domain, obtained as the Fourier transforms of those in the space domain, that those potentials must satisfy are given as

$$\tilde{\phi}_1(\alpha_n, h_2 + h_3) = \tilde{\phi}_2(\alpha_n, h_2 + h_3) \tag{4a}$$

$$\tilde{\phi}_1(\alpha_n, h_2 + h_3) = \tilde{V}^U(\alpha_n) \tag{4b}$$

$$\epsilon_{r1}\left.\frac{\partial^2\tilde{\phi}_2}{\partial y}\right|_{y=h_2+h_3} - \left.\frac{\partial\tilde{\phi}_1}{\partial y}\right|_{y=h_2+h_3} = \frac{\tilde{\rho}^U(\alpha_n)}{\epsilon_0} \tag{4c}$$

$$\tilde{\phi}_2(\alpha_n, h_3) = \tilde{\phi}_3(\alpha_n, h_3)) \tag{4d}$$

$$\tilde{\phi}_3(\alpha_n, h_3) = \tilde{V}^L(\alpha_n) \tag{4e}$$

$$\epsilon_{r2}\left.\frac{\partial\tilde{\phi}_3}{\partial y}\right|_{y=h_3} - \epsilon_{r1}\left.\frac{\partial\tilde{\phi}_2}{\partial y}\right|_{y=h_3} = \frac{\tilde{\rho}^L(\alpha_n)}{\epsilon_0} \tag{4f}$$

$$\tilde{V}^X(\alpha_n) = \tilde{V}_0^X(\alpha_n) + \tilde{V}_1^X(\alpha_n), \qquad X = U, L \tag{4g}$$

$$\frac{\tilde{\rho}^X(\alpha_n)}{\epsilon_0} = \frac{\tilde{\rho}_S^X(\alpha_n) + \tilde{\rho}_{g1}^X(\alpha_n) + \tilde{\rho}_{g2}^X(\alpha_n)}{\epsilon_0}, \qquad X = U, L \tag{4h}$$

where, in the above equations and in what follows, quantities with the subscripts U and L correspond to the upper and lower surfaces of the central substrate, respectively. $\tilde{V}_0^X$, $X = U, L$, represent the Fourier transforms of the known potentials of the strips, respectively; $\tilde{V}_1^X$ are the Fourier transforms of unknown potential distributions on the left- and right-hand-side slots; the ground planes are assumed to be at zero potential; $\tilde{\rho}_S^X$, $\tilde{\rho}_{g1}^X$, and $\tilde{\rho}_{g2}^X$ stand for the Fourier transforms of the unknown charge distributions of the strips, the left-hand-side ground planes, and the right-hand-side ground planes, respectively; ϵ_0 is the free-space permittivity; and ϵ_{r1} and ϵ_{r2} are the relative dielectric constants of the central and bottom substrates, respectively.

Imposing the foregoing boundary conditions then yields the following system of coupled linear algebraic equations

$$\tilde{G}_{11}(\alpha_n)\tilde{\rho}^U(\alpha_n) + \tilde{G}_{12}(\alpha_n)\tilde{\rho}^L(\alpha_n) = \tilde{V}^U(\alpha_n) \tag{5a}$$

$$\tilde{G}_{12}(\alpha_n)\tilde{\rho}^U(\alpha_n) + \tilde{G}_{22}(\alpha_n)\tilde{\rho}^L(\alpha_n) = \tilde{V}^L(\alpha_n) \tag{5b}$$

where the spectral-domain Green's functions, $\tilde{G}_{ij}$, $i = 1, 2$, and $j = 1, 2$, are derived as

$$\tilde{G}_{11} = \frac{1}{E}\left[\tanh \alpha_n h_1\left(\frac{\epsilon_{r2}}{\epsilon_{r1}}\tanh \alpha_n h_2 + \tanh \alpha_n h_3\right)\right] \tag{6a}$$

$$\tilde{G}_{12} = \tilde{G}_{21} = \frac{1}{E}\frac{\tanh \alpha_n h_1 \tanh \alpha_n h_3}{\cosh \alpha_n h_2} \tag{6b}$$

$$\tilde{G}_{22} = \frac{1}{E}\left[\tanh \alpha_n h_3\left(\tanh \alpha_n h_1 + \frac{1}{\epsilon_{r1}}\tanh \alpha_n h_2\right)\right] \tag{6c}$$

$$E = \epsilon_0\alpha_n \tanh \alpha_n h_2\left[\epsilon_{r2}\left(\frac{1}{\epsilon_{r1}} + \tanh \alpha_n h_1 \coth \alpha_n h_2\right) + \tanh \alpha_n h_3\,(\coth \alpha_n h_2 + \epsilon_{r1}\tanh \alpha_n h_1)\right]. \tag{6d}$$

Galerkin's method along with Parseval's theorem are now employed to solve equation (5). In order to do that, we first expand the unknown charge distributions as series in terms of known basis functions, and then substitute the series into (5) and take the inner products of the resulting equations with the individual basis functions. The result

is a system of $[M^U + M^L + 2(N^U + N^L)]$ coupled linear equations.

$$\sum_{m=1}^{M^U} P_{11}^{im}(\alpha_n)\, c_m^U + \sum_{p=1}^{N^U} P_{12}^{ip}(\alpha_n)\, d_{1p}^U + \cdots + \sum_{k=1}^{N^L} P_{16}^{ik}(\alpha_n)\, d_{2k}^L = Q_i^U, \quad i = 1, 2, \cdots, M^U \tag{7a}$$

$$\sum_{m=1}^{M^U} P_{21}^{jm}(\alpha_n)\, c_m^U + \sum_{p=1}^{N^U} P_{22}^{jp}(\alpha_n)\, d_{1p}^U + \cdots + \sum_{k=1}^{N^L} P_{26}^{jk}(\alpha_n)\, d_{2k}^L = O_{1j}^U, \quad j = 1, 2, \cdots, N^U \tag{7b}$$

$$\vdots$$

$$\sum_{m=1}^{M^U} P_{61}^{jm}(\alpha_n)\, c_m^U + \sum_{p=1}^{N^U} P_{62}^{jp}(\alpha_n)\, d_{1p}^U + \cdots + \sum_{k=1}^{N^L} P_{66}^{jk}(\alpha_n)\, d_{2k}^L = O_{2j}^L, \quad j = 1, 2, \cdots, N^L \tag{7c}$$

where c_m^U, $m = 1, 2, \cdots, M^U$, d_{1p}^U, $p = 1, 2, \cdots, N^U$, $\cdots$, and d_{2k}^L, $k = 1, 2, \cdots, N^L$, are unknown coefficients associated with the respective known Fourier-transformed known basis functions $\tilde{\rho}_{sm}^U$, $\tilde{\rho}_{g1p}^U$, $\cdots$, and $\tilde{\rho}_{g2k}^L$ that describe the charge distributions of the upper strip, the upper-left ground plane, $\cdots$, and the lower-right ground plane, respectively. For an exact computation, the series should be infinite. Here, for computational purposes, they are limited to M^X, $X = U, L$ and N^X for the strip and ground planes respectively. P's and Q's are known parameters obtained from the inner products. For instance,

$$P_{16}^{ik} = \sum_{n=1}^{\infty} \tilde{\rho}_{si}^U \tilde{G}_{12} \tilde{\rho}_{g2k}^L, \quad i = 1, 2, \cdots, M^U; \quad k = 1, 2, \cdots, N^L \tag{8}$$

$$Q_i^U = \frac{2V_0^U}{a} \int_{G+S}^{G+S+W} \rho_{si}^U(x)\, dx. \tag{9}$$

Equation (7) can now be solved for the unknown coefficients, from which the per-unit-length capacitances, C_e^X and C_o^X, $X = U, L$, corresponding to equal ($V_{0,e}^U = V_{0,e}^L = 1$) and opposite ($V_{0,o}^U = -V_{0,o}^L = 1$) potential excitations on the strips, respectively, can be computed from the relation

$$C_r^X = \frac{a}{2(V_{0,r}^X)^2} \sum_{m=1}^{M^X} c_m^X Q_m^X, \quad r = e, o \tag{10}$$

B. c- and π-Mode Quasi-Static Analysis

The charge equations for the coupled structures (Fig. 1) can be written as

$$Q^U = (C^{U0} + C^{UL}) V_0^U - C^{UL} V_0^L \tag{11a}$$

$$Q^L = -C^{UL} V_0^U + (C^{L0} + C^{UL}) V_0^L \tag{11b}$$

where Q^X and V_0^X, $X = U, L$, are the total charges and potentials on the strips, respectively; C^{X0} is the self-capacitance per unit length of the strip X; and C^{UL} is the mutual-capacitance per unit length between the upper and lower strips. Now we impose the following sets of excitations according to [11]:

(i) Even-symmetric excitation: $V_0^U = V_0^L = 1$

(ii) Odd-symmetric excitation: $V_0^U = -V_0^L = 1$

(iii) c-mode excitation: $V_0^U = 1$, $V_0^L = R_c$

(iv) π-mode excitation: $V_0^U = 1$, $V_0^L = R_\pi$

where $R_{c,\pi}$ stand for the ratios of the voltages on the strips for modes c and π [10].

For the even- and odd-symmetric excitations, we obtain the following relations

$$C^{U0} = C_e^U \tag{12a}$$

$$C^{L0} = C_e^L \tag{12b}$$

$$C^{UL} = \tfrac{1}{2}(C_o^U - C_e^U) = \tfrac{1}{2}(C_o^L - C_e^L). \tag{12c}$$

Finally, using the c- and π-mode excitations, along with (12), yields the quasi-static per-unit-length C_ν^X of strip X for mode ν, $\nu = c, \pi$, as

$$C_\nu^U = C_e^U + \frac{1}{2}(C_o^U - C_e^U)(1 - R_\nu) \tag{13a}$$

$$C_\nu^L = C_e^L + \frac{1}{2}(C_o^U - C_e^U)\left(1 - \frac{1}{R_\nu}\right). \tag{13b}$$

The voltage ratios $R_{c,\pi}$ can be evaluated from [12]

$$R_{c,\pi} = \frac{1}{2E_1}\{(D_2 - D_1) \mp [(D_2 - D_1)^2 + 4E_1E_2]^{1/2}\} \tag{14}$$

where

$$D_1 = \frac{c_{11}c_{022} - c_{12}c_{012}}{\det[c_0]}$$

$$D_2 = \frac{c_{22}c_{011} - c_{12}c_{012}}{\det[c_0]}$$

$$E_1 = \frac{c_{12}c_{022} - c_{22}c_{012}}{\det[c_0]}$$

$$E_2 = \frac{c_{12}c_{011} - c_{11}c_{012}}{\det[c_0]}$$

$$\det[c_0] = v_0^2(c_{011}c_{022} - c_{012}^2) \tag{15}$$

and v_0 is the free space velocity. c_{ij}, $i, j, = 1, 2$, are elements of the per-unit-length capacitance matrix of the structure and can be obtained, by making use of (13), as

$$c_{11} = \tfrac{1}{2}(C_e^U + C_o^U) \tag{16a}$$

$$c_{22} = \tfrac{1}{2}(C_e^L + C_o^L) \tag{16b}$$

$$c_{12} = \tfrac{1}{2}(C_e^U - C_o^U) = \tfrac{1}{2}(C_e^L - C_o^L). \tag{16c}$$

c_{0ij} are elements of the same capacitance matrix per unit length but with all the dielectric substrates replaced by air.

The mode characteristic impedances $Z_{0,\nu}^X$ and effective dielectric constants $\epsilon_{\text{eff},\nu}$ of the strips for modes ν can now be determined from the following formulas [12]:

$$Z_{0,\nu}^X = \frac{1}{v_\nu C_\nu^X} \tag{17}$$

$$\epsilon_{\text{eff},\nu} = \left(\frac{v_0}{v_\nu}\right)^2 \tag{18}$$

where v_ν, the phase velocities for modes ν, are given as

$$v_{c,\pi} = \left\{\frac{D_1 + D_2}{2} \mp \frac{1}{2}[(D_1 - D_2)^2 + 4E_1E_2]^{1/2}\right\}^{-1/2}. \tag{19}$$

When $h_1 = h_3$ and $\epsilon_2 = \epsilon_0$, the c- and π-modes in the FBCPW become the even- and odd-modes, respectively. That is, $Z_{0,c(\pi)}^U = Z_{0,c(\pi)}^L = Z_{0,e(o)}$, $\epsilon_{\text{eff},c(\pi)} = \epsilon_{\text{eff},e(o)}$, where $Z_{0,e(o)}$ and $\epsilon_{\text{eff},e(o)}$ are the even (odd) mode characteristic impedance and effective dielectric constant, respectively.

For the TBCPW (Fig. 1(b)), the derived Green's function remain the same. However, (8) is reduced to a set of $(M^U + M^L + 2N^U)$ equations.

III. Numerical Results

To obtain numerical results, we used the following basis functions

$$\rho_{sm}^U(x) = \rho_{sm}^L(x) = \frac{\cos\left[(m-1)\,\pi\,\dfrac{x - G - S}{W}\right]}{\left\{1 - \left[\dfrac{2(x - S - G) - W}{W}\right]^2\right\}^{1/2}} \tag{20a}$$

$$\rho_{g1m}^U(x) = \rho_{g1m}^L(x) = \frac{\cos\left[\left(m - \dfrac{1}{2}\right)\pi\,\dfrac{x - G}{G}\right]}{\left[1 - \left(\dfrac{x}{G}\right)^2\right]^{1/2}} \tag{20b}$$

$$\rho_{g2m}^U(x) = \rho_{g2m}^L(x) = \frac{\cos\left[\left(m - \dfrac{1}{2}\right)\pi\,\dfrac{x - a + G}{G}\right]}{\left[1 - \left(\dfrac{a - x}{G}\right)^2\right]^{1/2}} \tag{20c}$$

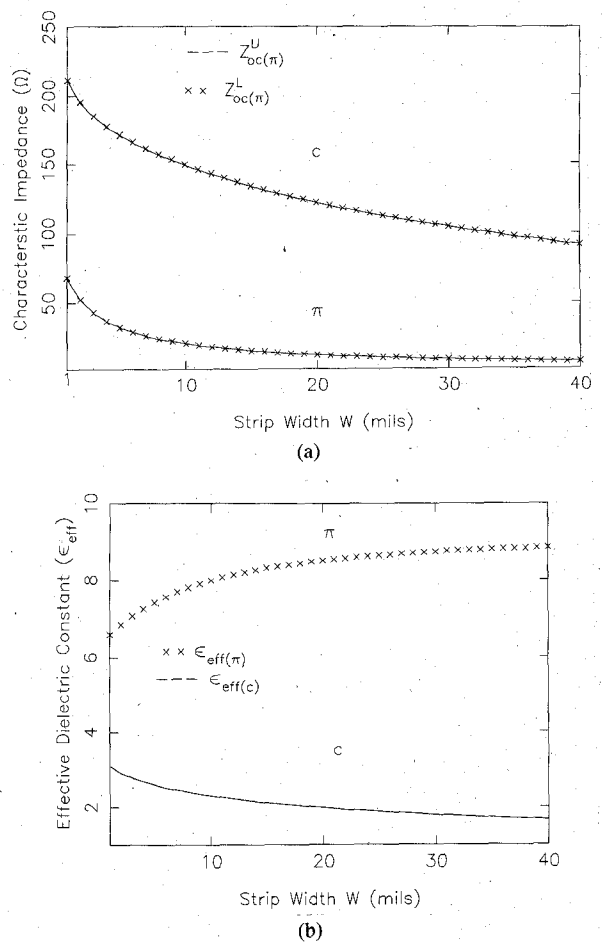

Fig. 3. Mode characteristic impedances (a) and effective dielectric constants (b) of the TBCPW versus the strip width. $a = 100$ mil, $h_1 = h_3 = 20$ mil, $h_2 = 5$ mil, $\epsilon_{r1} = 10.5$ (Alumina), $\epsilon_{r2} = 1$ (air), $S = 20$ mil.

which are defined only over the strips and left and right ground planes, respectively, and the charge density in (20b) and (20c) vanishes at $x = 0$ and $x = a$, respectively. $m = 1, 2, \cdots, M^X$, $X = U, L$, for ρ_{sm}^X and $m = 1, 2, \cdots, N^X$ for ρ_{g1m}^X and ρ_{g2m}^X. These functions describe closely the actual behavior of the charge distributions due to the inclusion of the edge effects. Their Fourier transforms are given in the Appendix.

Results of the c- and π-mode characteristic impedances and effective dielectric constants for the TBCPW and FBCPW are similar, so only those of the former are presented here. Fig. 3 shows calculated values of the c- and π-mode characteristic impedances and effective dielectric constants for the TBCPW versus the strip width. As can be seen, increasing the strip width reduces all the mode characteristic impedances while respectively increasing and decreasing the π- and c-mode effective dielectric constants, resulting in an increase for the effective-dielectric-constant ratio. Also, the TBCPW, while having similar π-mode characteristic impedances and effective dielectric constants as those for the FBCPW, has higher c-mode impedances, thus producing a larger impedance ratio. At $W = 40$ mil, impedance and effective-dielectric-constant ratios of more than 14 and 5 are obtained for the TBCPW,

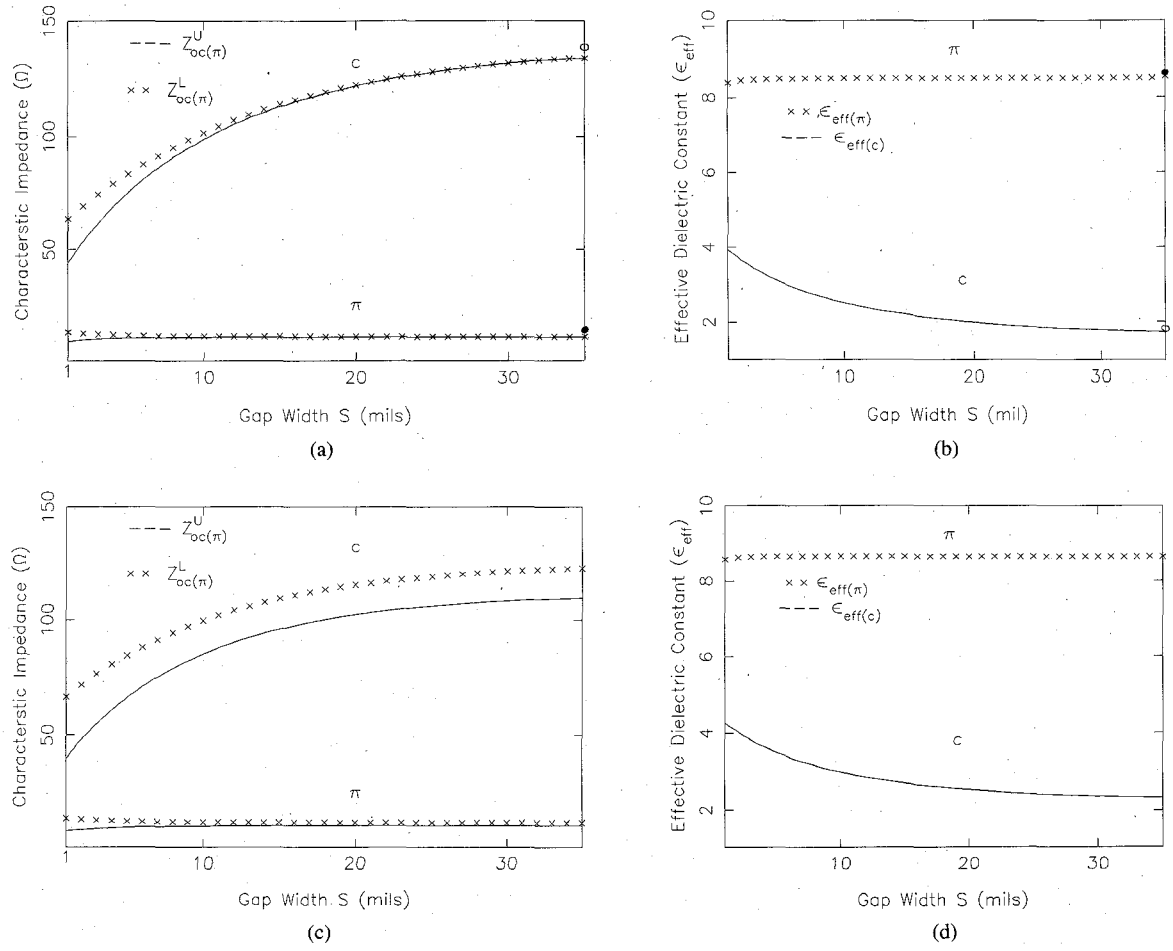

Fig. 4. Mode characteristic impedances (a), (c) and effective dielectric constants (b), (d) of the TBCPW versus the gap width. a = 100 mil, $h_1 = h_3$ = 20 mil, h_2 = 5 mil, ϵ_{r1} = 10.5 (Aluminia), W = 20 mil. (a), (b) ϵ_{r2} = 1 (air). (c), (d) ϵ_{r2} = 2.2 (Duroid). Open and filled circles represent the respective even- and odd-mode data, independent of the gap width, of the broadside-coupled strip-line.

respectively. These unique phenomena are very desirable for applications requiring broad bandwidth and tight coupling.

In Fig. 4, mode characteristic impedances and effective dielectric constants for the TBCPW are plotted as a function of the gap width. It is seen that as the gap width is increased the c-mode characteristic impedance and effective dielectric constant increases and decreases respectively, whereas those for the π-mode remain virtually the same. As a result, large ratios for the mode effective dielectric constants and characteristic impedances can be achieved by increasing the gap width. Again, the TBCPW has larger impedance ratio than the FBCPW due to higher c-mode impedance. At S = 35 mil, the TBCPW has impedance and effective-dielectric-constant ratios of about 11.5 and 5, respectively. It is also clear that as the dielectric constant of the lower substrate increases, the mode characteristic impedances and effective dielectric constants of the lower strip decrease while those of the upper strip remain virtually unaffected.

Fig. 5 shows variations of the mode characteristic impedances and effective dielectric constants of the TBCPW versus the gap width for unequal spacings between the substrate and the channel top and bottom walls. Compared to the equal-spacing data (Fig. 4), the ratio of the mode impedances increases due to an increase in the c-mode characteristic impedance of the upper strip, while that for the effective dielectric constants is virtually unchanged.

Computed values of the mode characteristic impedances and effective dielectric constants of the TBCPW are plotted against the channel width in Fig. 6. It is apparent that these parameters are insensitive with changes in the channel width. It should be noted, however, that although the channel width does not affect the transmission line characteristics, it must be appropriately chosen to avoid the propagations of the parallel-plate and higher-order modes at desired frequencies.

As an example to compare our new broadside-coupled CPWs to the familiar broadside-coupled strip-line, calculated characteristic impedances and effective dielectric constants of the latter, obtained using an analysis similar to the one presented in Section II, are also presented in Fig. 4(a)–(b). It is readily seen, as expected, that the results for the TBCPW approach those of the broadside-coupled strip-line as the gap width increases. One further

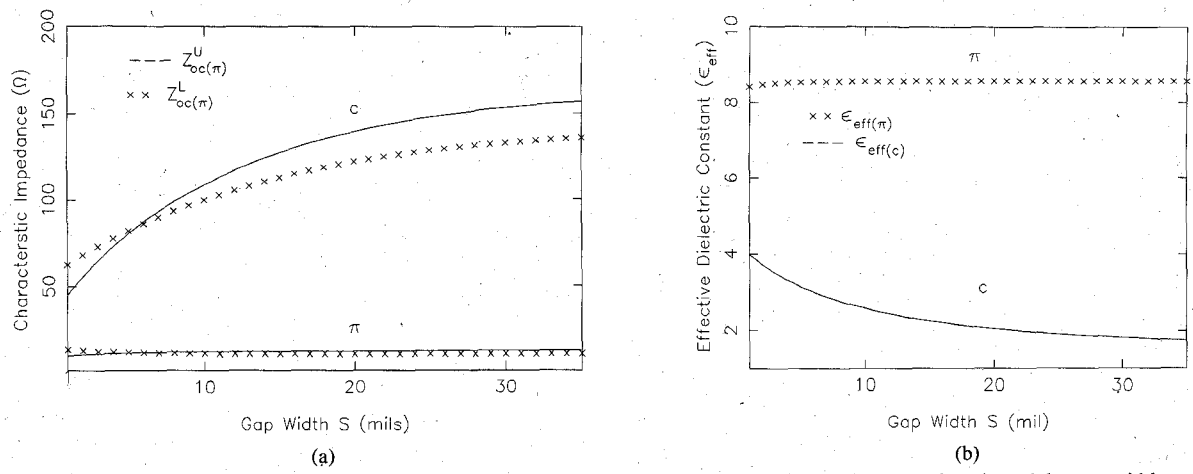

Fig. 5. Mode characteristic impedances (a) and effective dielectric constants (b) of the TBCPW as a function of the gap width. a = 100 mil, h_1 = 30 mil, h_2 = 5 mil, h_3 = 20 mil, ϵ_{r1} = 10.5 (Alumina), ϵ_{r2} = 1 (air), W = 20 mil.

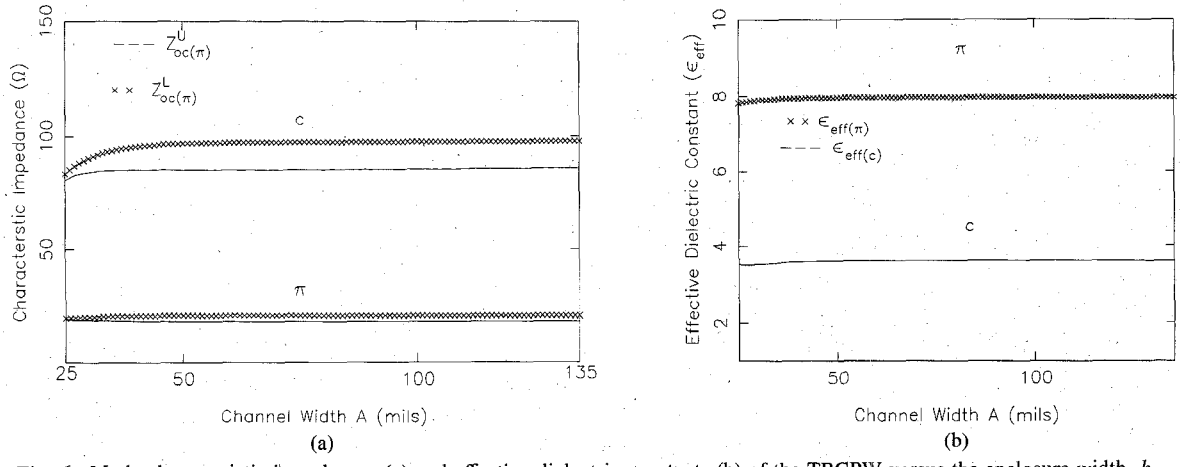

Fig. 6. Mode characteristic impedances (a) and effective dielectric constants (b) of the TBCPW versus the enclosure width, h_1 = h_3 = 20 mil, h_2 = 5 mil, ϵ_{r1} = 10.5 (Alumina), ϵ_{r2} = 1 (air), W = 10 mil, S = 5 mil.

remark appropriate here is that, compared to the broadside-coupled strip-line that has only one impedance set for a given strip width, CPW counterparts have a wide range of impedance values, which make them very useful for circuit designs where different impedance levels are needed.

IV. Filter Design and Performance

New end-coupled band-pass filters using the broadside-coupled CPWs, are shown in Fig. 2. They are actually a direct-coupled-resonator band-pass filter that consists of a sequence of CPW broadside coupled sections, periodically located along CPW. To demonstrate the performance of the proposed new filters and to validate the developed analyses of the broadside-coupled CPWs, two X-band (8–12 GHz) three-section filters, with a pass-band ripple of 0.4 dB, were designed and tested. The filter design was based on the mode characteristic impedances and effective dielectric constants of the FBCPW, TBCPW, and CPW. The filter theoretical responses were obtained through the use of the equivalent circuit of an open-circuited interdigital coupled-line section [13] and chain matrix of a transmission line section. The channel dimensions are a = 180 mil and b = 131 mil. The filters were fabricated on a Duriod substrate with a relative dielectric constant of 2.2 and a thickness of 31 mil. Figs. 7 and 8 show their performances. Insertion losses of less than 1.5 and 1.0 dB were achieved in the pass bands for the

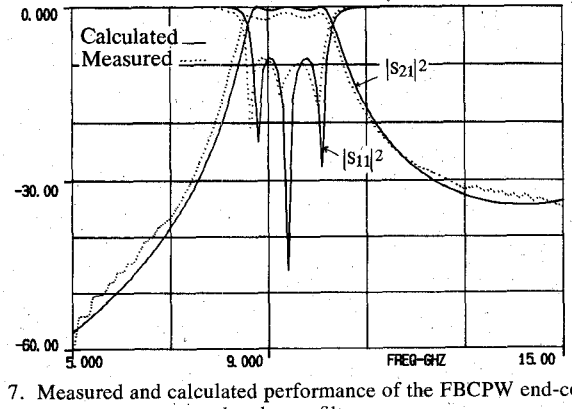

Fig. 7. Measured and calculated performance of the FBCPW end-coupled band-pass filter.

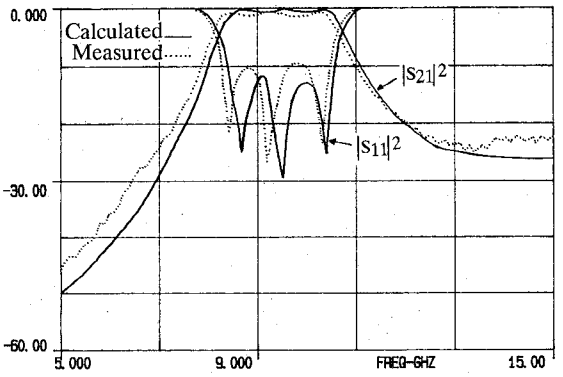

Fig. 8. Measured and computed performance of the TBCPW end-coupled band-pass filter.

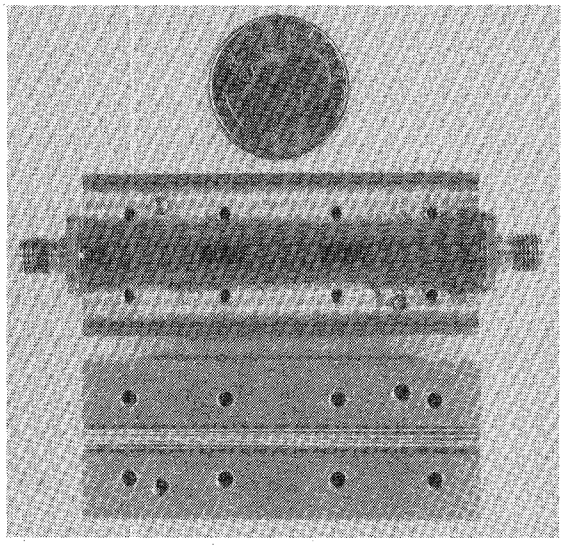

Fig. 9. A photograph of the FBCPW end-coupled band-pass filter.

FBCPW and TBCPW filters, respectively. It can be seen that there is a good agreement between the calculated and measured responses. A photograph of the filter, fabricated using the FBCPW, and its test fixture is given in Fig. 9.

V. Conclusions

New broadside-coupled CPWs, suitable for broad-band applications as well as those requiring tight couplings and large ratios of mode effective dielectric constants, along with their analyses have been presented. It has been found that ratios for the mode characteristic impedances and effective dielectric constants increase with increasing gap width. The effective-dielectric-constant ratio also increases with increasing strip width. By properly selecting the spacings between the substrate and the enclosure top and bottom walls, one can also realize large impedance ranges. The development of CPW broadside end-coupled band-pass filters has also been reported for the first time. The measured results obtained for three-resonator filters, fabricated using the TBCPW and FBCPW, in X-band are in good agreement with the computed performances, which validates the developed broadside-coupled CPW analyses. The TBCPW filter exhibits noticeably lower insertion loss than the FBCPW as expected. These new filter structures are attractive components in many narrow- as well as wide-band applications.

Appendix

Fourier transforms of the charge distributions described in (20) are derived as

$$\tilde{\rho}^{U}_{sm}(\alpha_n) = \tilde{\rho}^{L}_{sm}(\alpha_n) = \frac{\pi}{2}\frac{W}{a}\left\{J_0\left(\frac{m-1}{2}\pi + \alpha_n\frac{W}{2}\right)\cdot \sin\left[\frac{m-1}{2}\pi + \alpha_n\left(G+S+\frac{W}{2}\right)\right] - J_0\left(\left|\frac{m-1}{2}\pi - \alpha_n\frac{W}{2}\right|\right)\sin\left[\frac{m-1}{2}\pi - \alpha_n\left(G+S+\frac{W}{2}\right)\right]\right\}$$

$$\tilde{\rho}^{U}_{g1m}(\alpha_n) = \tilde{\rho}^{L}_{g1m}(\alpha_n) = \frac{\pi}{2}\frac{G}{a}\left\{\left(J_0\left[\left(m-\frac{1}{2}\right)\pi - \alpha_n G\right] - J_0\left[\left(m-\frac{1}{2}\right)\pi + \alpha_n G\right]\right)\cdot \sin\left(m-\frac{1}{2}\right)\pi - \left(H_0\left[\left(m-\frac{1}{2}\right)\pi - \alpha_n G\right] - H_0\left[\left(m-\frac{1}{2}\right)\pi + \alpha_n G\right]\right)\cdot \cos\left(m-\frac{1}{2}\right)\pi\right\}$$

$$\tilde{\rho}^{U}_{g2m}(\alpha_n) = \tilde{\rho}^{L}_{g2m}(\alpha_n) = \frac{\pi}{2}\frac{G}{a}\left\{J_0\left[\left(m-\frac{1}{2}\right)\pi + \alpha_n G\right]\cdot \sin\left[\left(m-\frac{1}{2}\right)\pi + \alpha_n a\right] - J_0\left[\left(m-\frac{1}{2}\right)\pi - \alpha_n G\right]\sin\left[\left(m-\frac{1}{2}\right)\pi - \alpha_n a\right] - H_0\left[\left(m-\frac{1}{2}\right)\pi + \alpha_n G\right]\cos\left[\left(m-\frac{1}{2}\right)\pi + \alpha_n a\right] + H_0\left[\left(m-\frac{1}{2}\right)\pi - \alpha_n G\right]\cdot \cos\left[\left(m-\frac{1}{2}\right)\pi - \alpha_n a\right]\right\}$$

where J_0 and H_0 denote the zeroth-order Bessel function of the first kind and Struve function, respectively.

Acknowledgment

The author wishes to thank Dr. A. D. Patton and Dr. T. R. Lalk for their constant encouragement and Messrs. M. Tran and L. Fan for their technical support. The author would also like to thank an anonymous reviewer for many useful comments.

REFERENCES

[1] J. E. Dalley, "A strip-line directional coupler utilizing a non-homogeneous dielectric medium," *IEEE Trans. Microwave Theory Tech.*, vol. MTT-17, pp. 706–712, Sept. 1969.

[2] J. L. Allen and M. F. Estes, "Broadside-coupled strips in a layered dielectric medium," *IEEE Trans. Microwave Theory Tech.*, vol. MTT-20, pp. 662–669, Oct. 1972.

[3] J. L. Allen, "Inhomogeneous coupled-line filters with large mode-velocity ratios," *IEEE Trans. Microwave Theory Tech.*, vol. MTT-22, pp. 1182–1186, Dec. 1974.

[4] T. Hatsuda, "Computation of coplanar-type strip-line characteristics by relaxation method and application to microwave circuits," *IEEE Trans. Microwave Theory Tech.*, vol. MTT-23, pp. 795–802, Oct. 1975.

[5] S. S. Bedair and I. Wolff, "Fast and accurate analytic formulas for calculating the parameters of a general broadside-coupled coplanar waveguide for (M)MIC applications," *IEEE Trans. Microwave Theory Tech.*, vol. 37, pp. 843–850, May 1989.

[6] T. Itoh and A. S. Hebert, "A generalized spectral domain analysis for coupled suspended microstriplines with tuning septums," *IEEE Trans. Microwave Theory Tech.*, vol. MTT-26, pp. 820–826, Oct. 1978.

[7] D. F. Williams and S. E. Schwarz, "Design and performance of coplanar waveguide bandpass filters," *IEEE Trans. Microwave Theory Tech.*, vol. MTT-31, pp. 558–566, July 1983.

[8] N. I. Dib, L. P. B. Katehi, G. E. Ponchak, and R. N. Simons, "Theoretical and experimental characterization of coplanar waveguide discontinuities for filter applications," *IEEE Trans. Microwave Theory Tech.*, vol. 39, pp. 873–882, May 1991.

[9] Y. H. Shu, J. A. Navarro, and K. Chang, "Electronically switchable and tunable coplanar waveguide-slotline band-pass filters," *IEEE Trans. Microwave Theory Tech.*, vol. 39, pp. 548–554, Mar. 1991.

[10] V. K. Tripathi, "Asymmetric coupled transmission lines in an inhomogeneous medium," *IEEE Trans. Microwave Theory Tech.*, vol. MTT-23, pp. 734–739, Sept. 1975.

[11] C. Nguyen, "Millimeter-wave spur-line band-stop filters in an inhomogeneous medium," M.S. thesis, California State University, Northridge, 1983.

[12] C. Nguyen and K. Chang, "On the analysis and design of spurline bandstop filters," *IEEE Trans. Microwave Theory Tech.*, vol. MTT-33, pp. 1416–1421, Dec. 1985.

[13] V. K. Tripathi, "Equivalent circuits and characteristics of inhomogeneous nonsymmetrical coupled-line two-port circuits," *IEEE Trans. Microwave Theory Tech.*, vol. MTT-25, pp. 140–142, Feb. 1977.

Cam Nguyen (S'82–M'83–SM'91) received the B.S. degree in Mathematics from the National University of Saigon, Vietnam, and the B.S., M.S., and Ph.D. degrees in electrical engineering from the California Polytechnic University, Pomona, the California State University, Northridge, and the University of Central Florida, respectively.

Before joining the faculty of the Department of Electrical Engineering of the Texas A&M University in December 1990, he was employed from 1979 to 1990 by TRW, Hughes Aircraft, Aerojet ElectroSystem and ITT companies in California, and Martin Marietta in Florida, where he worked in many microwave and millimeter-wave R&D projects. He has developed many MIC and MMIC components and subsystems up to 170 GHz using diodes, MESFETs, HEMTs and HBTs.

Dr. Nguyen has published over 35 papers and two book chapters and is listed in Who's Who in America, Who's Who of Emerging Leaders in America, and Who's Who in the West. His current research interests are in the area of microwave and millimeter-wave circuits and devices.